Numerical Investigation of Turbulent Flow Using LES Turbulence Model

*Naman Agarwal

Abstract

Turbulence is primarily used in industrial applications as it induces mixing. The understanding of the dynamics is essentially required for better equipment design. Hence the present work focuses on numerical modeling of turbulent flow in a pipe using large eddy simulation (LES) turbulence model for range of Reynolds numbers. The LES model inherently resolves large scales of motion and filters out the small universal scales. The numerical results are compared and also validated against the commercial software ANSYS Fluent 18.0. The model predicted the flow behaviour accurately for a range of Reynolds number.

Keywords: Turbulence, Pipe flow, Large eddy simulation, Finite element method

Introduction

Turbulence produces highly chaotic movement with variation in velocity and pressure. The understanding of turbulence is necessary as it plays a major role in many industrial applications. Hence, numerical modeling is essentially required which provides ample amount of information of the flow fields which is difficult to obtain through experiments. The present work focuses LES model verification for various Reynolds number and its verification against a commercial software ANSYS Fluent 18.0. A simple 2D pipe is used in the present work to analyze the flow behavior.

In the past, numerous works have been performed to model turbulence in a pipe. The turbulence models currently used in the industry, namely the Reynolds-averaged Navier Stokes equation (RANS) models, have limited accuracy due to its simplifying assumptions. Flow in a pipe was studied throgh experiments by Abbott & Kline (1962) for a Reynolds number of 4:0 x 105. The velocity profile matched well with the turbulent at plate profile. Barbin & Jones (1963) performed a similar study and found that the profile attained a logarithmic distribution.

Adrian et al. (1994) compared the DNS and experimental data for Re = 7000 and contradicted the previous works by finding a profile which exceeded the logarithmic distribution. The variation was significantly increased near the center of the pipe. Other studies confirmed the accuracy of power law for the velocity profile in turbulent regime in a pipe (Le et al., 1997; Ould-Rouis & Feiz, 2009).

The effect of Reynolds number on mean flow velocity profiles in a smooth pipe was extensively studied and showed experimentally that the slope of logarithmic profile varies with the Reynolds number in the turbulent regime upto Re = 25000 (Den Toonder & Nieuwstadt, 1997). Hence, the ow pro_les developed in pipe vary for the same Reynolds number and needs to be numerically confirmed for a range of Reynolds number.

This paper is structured as follows. Section 2.1 presents the discussion on the basic governing equations of turbulent flow. Further, Section 2.2 discusses the finite element formulation of the flow equations. Section 3 describes the simulation setup of a 2-D pipe along with the initial and boundary conditions. The physical and numerical parameters are also described here. Section 4 discusses the results obtained. Initially, the effect of Reynolds number on flow behaviour is presented for 4 different Reynolds number. Further, the numerical solution was verified in an commercial finite volume software ANSYS Fluent 18.0. Finally, Section 5 concludes the paper with a summary of findings obtained from different simulations performed for the 2-D pipe for turbulent regime.

Methodology

2.1. Flow equations The basic momentum equation is defied as:

$$\frac{\partial \mathbf{u}_i}{\partial t} + \mathbf{u}_i \cdot \nabla \mathbf{u}_i = -\frac{1}{\rho}\nabla p + \nabla \cdot [\bar{\bar{\tau}}_i], \qquad (1)$$

where u_i is the phase velocity in spatial direction, ρ is the density, p is the static pressure, $[\bar{\bar{T}}_i]$is the shear stress tensor. The smaller spatial scales require a very fine mesh to resolve and hence are modeled. LES works on the principle of filtered decomposition which resolves the large anisotropic eddies and models the small universal eddies. The _ltered and the sub-_ltered components are given by (Bull, 2013):

$$\overline{\mathbf{u}} = G \star \mathbf{u}(\mathbf{x}, t) = \int_{-\infty}^{\infty} G(\mathbf{r})\mathbf{u}(\mathbf{x}-\mathbf{r}, t)d\mathbf{r}, \qquad (2)$$

$$\mathbf{u} = \overline{\mathbf{u}} + \mathbf{u}', \qquad (3)$$

Here, G(r) is the filter kernel and r is the radial distance that is associated with the filter. The stress due to sub-filtered interactions is known as the sub-filter-scale (SFS) stress whose spherical part is added to the pressure field, which results in a modified pressure field, $\bar{\bar{p}}$, and the deviatoric part, $[\bar{\bar{T}}_i]$ SFS i tensor, is retained in the equation and is modeled. The resulting filtered momentum equation for phase i is given as:

$$\frac{\partial \overline{\mathbf{u}}_i}{\partial t} + \overline{\mathbf{u}}_i \cdot \nabla \overline{\mathbf{u}}_i = -\frac{1}{\rho}\nabla \bar{\bar{p}} + \nabla \cdot [(\bar{\bar{\tau}}_i + \bar{\bar{\tau}}_i^{\mathrm{SFS}})], \quad (4)$$

SFS stress is modeled using the Boussinesq eddy viscosity hypothesis which is given as:

$$\bar{\bar{\tau}}^{\mathrm{SFS}} = -2\nu_T \bar{\bar{S}}, \quad (5)$$

where

$$\bar{\bar{S}} = \frac{1}{2}\left(\nabla \overline{\mathbf{u}} + (\nabla \overline{\mathbf{u}})^T\right). \quad (6)$$

Here ν_T is the eddy viscosity, a flow property, which is obtained using an eddy viscosity model in LES. The second-order Smagorinsky eddy viscosity model was used in the present work and discussed next.

Second-order Smagorinsky model

A balance is assumed between the production and the dissipation rate of SFS kinetic energy in the second-order Smagorinsky model (Smagorinsky, 1963). The eddy viscosity (ν_T) in this model is formulated as:

$$\nu_T = C_s^2 \overline{\Delta}^2 |\overline{S}|, \quad (7)$$

where C_s is the Smagorinsky constant and [S] is the rate of strain modulus, defined as:

$$|\overline{S}| = \sqrt{2\bar{\bar{S}} : \bar{\bar{S}}}. \quad (8)$$

The value of Cs varies between 0:1 to 0:17 for shear flows to satisfy the Kolmogorov -5/3 energy law (Pope, 2000).

2.2. Finite element formulation

The SFS stress term is modeled using the Boussinesq eddy viscosity hypothesis leading to the modeled equation as:

$$\frac{\partial \overline{\mathrm{u}}}{\partial t} + \overline{\mathrm{u}} \cdot \nabla \overline{\mathrm{u}} = -\frac{1}{\rho}\nabla \bar{\tilde{p}} + (\nu + \nu_T)\nabla^2 \overline{\mathrm{u}}. \quad (9)$$

A weak form of the filtered momentum equation is derived by "multiplying" it with a test function ew and integrating it over the volume, Ω resulting in:

$$\int_\Omega \tilde{w} \cdot \left(\frac{\partial \overline{\mathrm{u}}}{\partial t} + \overline{\mathrm{u}} \cdot \nabla \overline{\mathrm{u}} + \frac{1}{\rho}\nabla \bar{\tilde{p}} - (\nu + \nu_T)\nabla^2 \overline{\mathrm{u}}\right) \mathrm{d}\Omega = 0.$$

In the Galerkin FE method, velocity trial and test functions are approximated using the same bases, ϕ_l, as:

$$\overline{\mathbf{u}} = \sum_{l=1}^{N_{\text{nodes}}} (\overline{u}_l^1 \phi_l \widehat{\mathbf{i}} + \overline{u}_l^2 \phi_l \widehat{\mathbf{j}}) = \sum_{l=1}^{N_{\text{nodes}}} \phi_l \mathbf{u}_l, \qquad (11)$$

and

$$\widetilde{w} = \sum_{l=1}^{N_{\text{nodes}}} (\widetilde{w}_l^1 \phi_l \widehat{\mathbf{i}} + \widetilde{w}_l^2 \phi_l \widehat{\mathbf{j}}) = \sum_{l=1}^{N_{\text{nodes}}} \phi_l w_l. \qquad (12)$$

The basis functions $\emptyset_l$ take a value one at the node l and zero at all other nodes. In the continuous Galerkin (CG) approach, the chosen basis functions are continuous across elements. For illustration, Figure 1 shows continuous piecewise-linear functions for one dimensional (1-D) and 2-D meshes.

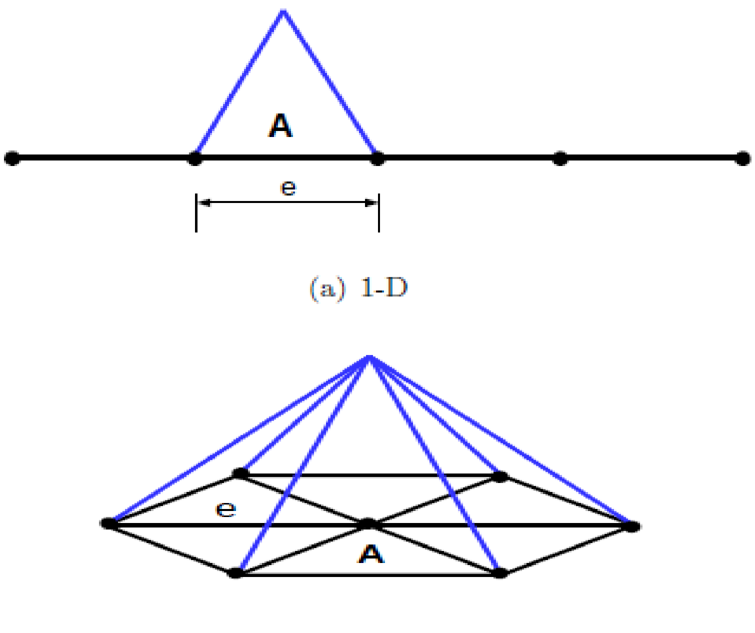

(b) 2-D

Figure 1: Piecewise-linear continuous finite element basis function with the adjacent nodes is shown for 1-D and 2-D meshes (figure adapted from Wilson (2009).

$$M\frac{\mathrm{d}\underline{\mathbf{u}}}{\mathrm{d}t} + A(\overline{\mathrm{u}})\underline{\mathrm{u}} + C\underline{\mathrm{p}} + K\underline{\mathrm{u}} = 0, \qquad (13)$$

where the mass matrix M, advection matrix A, pressure gradient matrix C and viscosity matrix K are given by:

$$M = \int_{\Omega} \phi_k \phi_l \mathrm{d}\Omega, \qquad (14)$$

$$A(\mathbf{u}) = -\int_{\Omega} \phi_l \overline{\mathbf{u}} \cdot \nabla \phi_k \mathrm{d}\Omega, \qquad (15)$$

$$C = \int_{\Omega} \frac{1}{\rho} \phi_k \nabla \varphi_l \mathrm{d}\Omega, \qquad (16)$$

$$K = \int_{\Omega} (\nu + \nu_T)(\nabla \phi_k \cdot \nabla \phi_l) \mathrm{d}\Omega. \qquad (17)$$

Simulation setup

The Reynolds number in pipe flow simulations is defined as:

$$Re = \frac{\mathrm{uD}}{\nu}, \qquad (18)$$

where u is the mean velocity in the x-direction developed in the pipe, ν is the kinematic viscosity of the fluid and D is the diameter of the pipe.

The geometry of pipe is schematically represented in Figure 2. The length (L) was sufficiently long for the flow to develop completely.

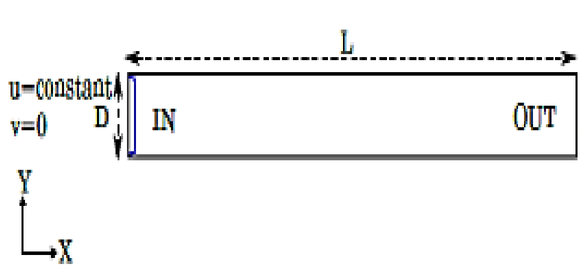

Figure 2: 2D geometry used in pipe flow simulation. L=200 mm and D=5:2 mm.

The boundary conditions applied in pipe flow simulations are specified in Table 1.

Table 1: Boundary conditions for 2D pipe flow simulation.

Boundary	Velocity	Pressure
Inlet	u=uniform,v=0	$\frac{\partial p}{\partial n} = 0$
Walls	No slip	$\frac{\partial p}{\partial n} = 0$
Outlet	$\frac{\partial u}{\partial n} = \frac{\partial v}{\partial n} = 0$	p=0

A no-slip boundary condition at the walls and a homogeneous Neumann condition for velocities at the outlet was applied. The flow velocity was initialized to zero for all simulations.

Table 2: Physical parameters for calculating inlet velocity in a 2D pipe flow simulation.

Physical parameter	Value
Reynolds number (Re)	7000
Density ($\mathrm{kg\,m^{-3}}$)	1.225
Diameter (m)	5.2×10^{-3}
Dynamic viscosity ($\mathrm{Pa \cdot s}$)	1.7894×10^{-5}

Table 3: Numerical parameters for 2D pipe flow simulation.

Numerical parameter	Value
Overall simulation time (s)	20
Number of Picard iterations	2
Tolerance for Picard iterations (L^2-norm)	10^{-12}

The physical parameters chosen in the Fluidity framework for current study are stated in Table 2. The numerical parameters are listed in Table 3. An implicit scheme was used with a maximum Courant-Friedrichs-Lewy (CFL) number of 0:5 for the simulations. All simulations were executed on a multicore machine with 20 threads to save on computation time.

4. Results and discussion

4.1. Effect of Reynolds number

The grid independence test conformed the use of FM2 mesh with nearly 54000 node points and mesh size of 0.16 mm. The pipe flow simulations were performed for a series of Reynolds number belonging to transition and turbulent regimes. The geometry and mesh details of different cases are discussed in Table 4 and Table 5, respectively.

Table 5: Mesh details of different cases in 2D pipe flow simulations.

Reynolds number (Re)	Mesh size (Δ x)(mm)	Nodes	Factor ($\frac{\Delta x}{\eta}$)
5000	0.16	51928	18.3
6000	0.16	53116	21
8000	0.16	55727	26

Figure 3 shows the velocity profiles at different sections in the domain for various Reynolds numbers. The profile obtained was attar in most of the region with high gradient on the walls. The magnitude of velocity increased with the Reynolds number, as seen in Figure 4. The atness of the profile increased with the Reynolds number. Hence, the flow dynamics was captured successfully for a range of Reynolds number.

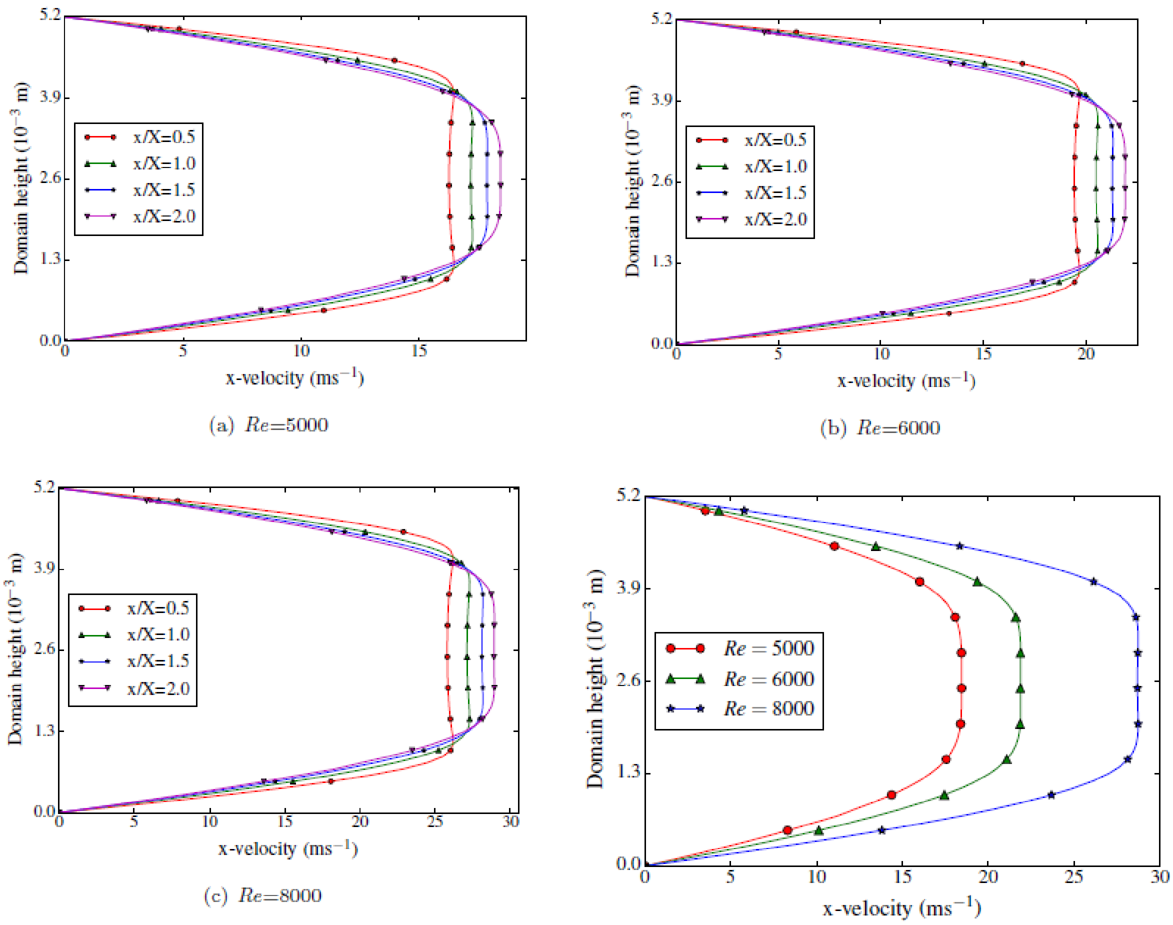

(a) Re=5000 (b) Re=6000 (c) Re=8000

Figure 4: Comparison of velocity profiles for various Reynolds numbers at x/X =2.0 in a pipe.

4.2. Benchmarking with ANSYS Fluent

The pipe ow simulations were also performed in the commercial finite volume solver ANSYS Fluent code for the FM2 mesh and the results were compared

against Fluidity. The aim of this study was investigate the accuracy of the open-source code used in the present work.

Table 6: Details of different options chosen in ANSYS Fluent for pipe flow simulation

Category	Details	Classification
Solver	Pressure based	
	Transient	
Model	Viscous	LES (Smagorinsky-Lilly)

.

The boundary conditions implemented in Fluent were the same as used in Fluidity. The details of LES options chosen in ANSYS Fluent are listed in Table 6. The solution methods used are listed in Table 7. The meshes imported in ANSYS Fluent were the same as presented previously.

Table 7: Details of different options chosen in solution methods for ANSYS Fluent pipe flow simulation.

Category	Details	Classification
P-V coupling	PISO	
Discretization	Gradient	Green-Gauss cell based
	Pressure	Second order
	Momentum	Bounded central differencing
Temporal formulation	Bounded second order implicit	
Under Relaxation factor	Pressure	0.3
	Density	1
	Body Force	1
	Momentum	0.7

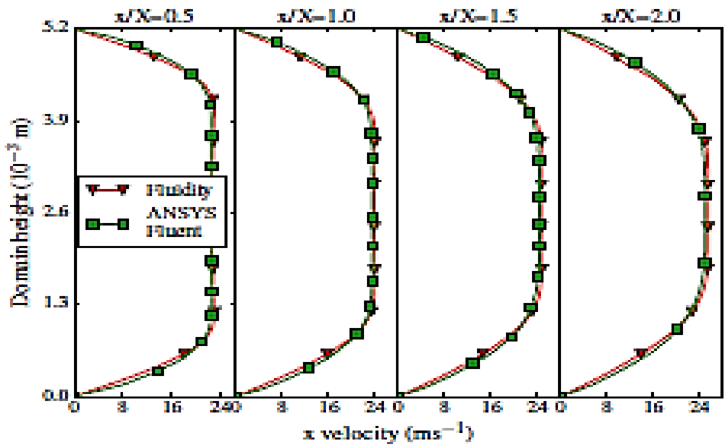

Figure 5: Comparison of velocity profiles for different solvers using LES turbulence model for FM2 mesh.

Figure 5 shows the velocity profiles of LES model at different sections in the pipe domain for FM2 mesh.

The flow profiles matched well in both the solvers: ANSYS Fluent and Fluidity. The relative change in the velocity profiles at the center of the domain using FM2 mesh was 0:7% at x/X=2:0. Hence, the excellent benchmarking results with ANSYS Fluent 18.0 conformed the accuracy of LES model implemented in Fluidity.

Conclusion

Turbulence modeling in a 2D pipe was presented in the work for Reynolds number of 7000. The flow profiles were initially analysed for a range of Reynolds numbers and showed a similar velocity profile with variation in a maximum velocity conforming the same behaviour of the LES model. Further, FEM results were verified with a commercial FVM software ANSYS Fluent 18 and results showed a promising match. Hence, LES captured turbulence dynamics for a range of Reynolds numbers and worked well in both FVM and FEM discretization's.

Nomenclature

2-D	two dimensional
CFD	computational fluid dynamics

CFL	Courant-Friedrichs-Lewy
CG	continuous Galerkin
FE	finite element
HPC	High-performance computing
LES	large eddy simulation
RANS	Reynolds-averaged Navier Stokes
SFS	sub-filter-scale

Uppercase Roman Symbols

A	advection matrix
C	pressure gradient matrix
$C\mu$	RANS model constant
C_s	Smagorinsky constant
$G_{(r)}$	filter kernel
K	viscosity matrix
L	Length of the domain
M	mass matrix
[S]	rate of strain modulus
$\bar{S}$	ltered rate of strain tensor

Lower Roman Symbols

k	turbulent kinetic energy
p	hydrostatic pressure
$\overline{p}$	modified pressure
r	radial distance associated with the filter
u	velocity
$\bar{u}$	filtered velocity
u'	fluctuating velocity
$\breve{w}$	test function

Greek Symbols

ϵ	energy dissipation rate
μ_t	eddy viscosity calculated using RANS model
ν_T	eddy viscosity
$\emptyset l$	Basis function of velocity
ρ	Density
$\bar{T}$	Shear stress tensor
$\bar{T}^{SFS}$	deviatoric part of SFS tensor
Δx	mesh size
Δ	Filter width
Ω	Computational domain

Mathematical symbols

:	Double dot product of two tensors
.	Dot product
∇	Gradient operator
*	Convolution operator

***Research Scholar,**
Multiphase Flow Research Lab,
Indian Institute of Technology Mandi

References

1. Abbott, D. E., & Kline, S. J. (1962). Experimental investigation of subsonic turbulent flow over single and double backward facing steps. Journal of Fluids Engineering, Transactions of the ASME, 84, 317-325.
2. Adrian, R. J., Friedrich, R., & Nieuwstadt, F. T. (1994). Fully developed turbulent pipe flow: A comparison between direct numerical simulation and experiment. Journal of Fluid Mechanics, 268, 175-210.

3. Barbin, A. R., & Jones, J. B. (1963). Turbulent flow in the inlet region of a smooth pipe. Journal of Fluids Engineering, Transactions of the ASME, 85, 29-33.doi:10.1115/1.3656521.

4. Bull, J. (2013). Turbulence Models with Adaptive Meshing for Industrial CFD. Ph.D. thesis Imperial College London.

5. Den Toonder, J. M., & Nieuwstadt, F. T. (1997). Reynolds number effects in a turbulent pipe flow for low to moderate Re. Physics of Fluids, 9, 3398-3409.

6. Le, H., Moin, P., & Kim, J. (1997). Direct numerical simulation of turbulent flow over a backward-facing step. Journal of Fluid Mechanics, 330, 349-374.

7. Ould-Rouis, M., & Feiz, A. (2009). Numerical simulation of turbulent pipe flow. Fluid Mechanics and Pipe Flow, 127, 231-267.

8. Pope, S. B. (2000). Turbulent ows. Cambridge University Press.

9. Smagorinsky, J. (1963). General circulation experiments with the primitive equations. Monthly Weather Review, 91, 99-164.

10. Wilson, C. (2009). Modelling multiple-material flows on adaptive unstructured meshes. Ph.D. thesis Imperial College London.